
Regulation of inorganic carbon acquisition in a red tide alga (*Skeletonema costatum*): the importance of phosphorus availability

Guang Gao^{a,b}, Jianrong Xia^{a*}, Jinlan Yu^a, Jiale Fan^b, Xiaopeng Zeng^a

^aSchool of Environmental Science and Engineering, Guangzhou University,
Guangzhou, 510006, China

^bMarine Resources Development Institute of Jiangsu, Huaihai Institute of Technology,
Lianyungang, 222005, China

*Corresponding author, Email: jrxia@gzhu.edu.cn; Phone: +86 (0)20 39366941; Fax:
+86 (0)20 39366949

1 Abstract:

2 *Skeletonema costatum* is a common bloom-forming diatom and encounters eutrophication and
3 severe carbon dioxide (CO₂) limitation during red tides. However, little is known regarding
4 the role of phosphorus (P) in modulating inorganic carbon acquisition in *S. costatum*,
5 particularly under CO₂ limitation conditions. We cultured *S. costatum* under five phosphate
6 levels (0.05, 0.25, 1, 4, 10 μmol L⁻¹) and then treated it with two CO₂ conditions (2.8 and 12.6
7 μmol L⁻¹) for two hours. The lower CO₂ reduced net photosynthetic rate at lower phosphate
8 levels (< 4 μmol L⁻¹) but did not affect it at higher phosphate levels (4 and 10 μmol L⁻¹). In
9 contrast, the lower CO₂ induced higher dark respiration rate at lower phosphate levels (0.05
10 and 0.25 μmol L⁻¹) and did not affect it at higher phosphate levels (> 1 μmol L⁻¹). The lower
11 CO₂ did not change relative electron transport rate (rETR) at lower phosphate levels (0.05 and
12 0.25 μmol L⁻¹) and increased it at higher phosphate levels (> 1 μmol L⁻¹). Photosynthetic CO₂
13 affinity (1/K_{0.5}) increased with phosphate levels. The lower CO₂ did not affect photosynthetic
14 CO₂ affinity at 0.05 μmol L⁻¹ phosphate but enhanced it at the other phosphate levels. Activity
15 of extracellular carbonic anhydrase was dramatically induced by the lower CO₂ at phosphate
16 replete conditions (> 0.25 μmol L⁻¹) and the same pattern also occurred for redox activity of
17 plasma membrane. Direct bicarbonate (HCO₃⁻) use was induced when phosphate
18 concentration was more than 1 μmol L⁻¹. These findings indicate P enrichment could enhance
19 inorganic carbon acquisition and thus maintain the photosynthesis rate in *S. costatum* grown
20 under CO₂ limiting conditions via increasing activity of extracellular carbonic anhydrase and
21 facilitating direct HCO₃⁻ use. This study sheds light on how bloom-forming algae cope with
22 carbon limitation during the development of red tides.

-
- 23 **Keywords:** carbonic anhydrase; CO₂ concentrating mechanisms; pH compensation point;
- 24 photosynthesis; redox activity; respiration

25 1. Introduction

26 Diatoms are unicellular photosynthetic microalgae that can be found worldwide in
27 freshwater and oceans. Marine diatoms account for 75% of the primary productivity for
28 coastal and other nutrient-rich zones and approximately 20% of global primary production
29 (Field *et al.*, 1998; Falkowski, 2012), hence playing a vital role in the marine biological
30 carbon pump as well as the biogeochemical cycling of important nutrients, such as nitrogen
31 and silicon (Nelson *et al.*, 1995; Moore *et al.*, 2013; Young & Morel, 2015). Diatoms usually
32 dominate the phytoplankton communities and form large-scale blooms in nutrient-rich zones
33 and upwelling regions (Bruland *et al.*, 2001; Anderson *et al.*, 2008; Barton *et al.*, 2016).
34 Nutrient enrichment is considered as a key factor that triggers algal blooms albeit the
35 occurrence of diatom blooms may be modulated by other environmental factors, such as
36 temperature, light intensity, salinity, and so forth (Smetacek & Zingone, 2013; Jeong *et al.*,
37 2015). When inorganic nitrogen and phosphorus are replete, diatoms can out-compete
38 chrysophytes, raphidophytes and dinoflagellates (Berg *et al.*, 1997; Jeong *et al.*, 2015; Barton
39 *et al.*, 2016) and dominate algal blooms due to their quicker nutrient uptake and growth rate.

40 In normal natural seawater (pH 8.1, salinity 35), HCO_3^- is the majority (~90%) of total
41 dissolved inorganic carbon (DIC, 2.0–2.2 mM). CO_2 (1%, 10–15 μM), which is the only
42 direct carbon source that can be assimilated by all photosynthetic organisms, only accounts
43 for 1% of total dissolved inorganic carbon. Diatoms' ribulose-1,5-bisphosphate
44 carboxylase/oxygenase (Rubisco), catalyzing the primary chemical reaction by which CO_2 is
45 transformed into organic carbon, has a relatively low affinity for CO_2 and is commonly less
46 than half saturated under current CO_2 levels in seawater (Hopkinson & Morel, 2011),

47 suggesting that CO₂ is limiting for marine diatoms' carbon fixation. To cope with the CO₂
48 limitation in seawater and maintain a high carbon fixation rate under the low CO₂ conditions,
49 diatoms have evolved various inorganic carbon acquisition pathways and CO₂ concentrating
50 mechanisms (CCMs), for instance, active transport of HCO₃⁻, the passive influx of CO₂,
51 multiple carbonic anhydrase (including both common (α , β , γ) and unusual (δ , ζ) families that
52 carries out the fast interconversion of CO₂ and HCO₃⁻), assumed C4-type pathway (using
53 phosphoenolpyruvate to capture more CO₂ in the periplastidal compartment), to increase the
54 concentration at the location of Rubisco and thus the carbon fixation. (Hopkinson & Morel,
55 2011; Hopkinson *et al.*, 2016). *Skeletonema costatum* is a worldwide diatom species that can
56 be found from equatorial to polar waters. It usually dominates large-scale algal blooms in
57 eutrophic seawaters (Wang, 2002; Li *et al.*, 2011). When blooms occur, seawater pH increases
58 and CO₂ decreases because the dissolution rate of CO₂ from the atmosphere cannot catch up
59 with its removal rate caused by intensive photosynthesis of algae. For instance, pH level in
60 the surface waters of the eutrophic Mariager Fjord, Denmark, could be up to 9.75 during algal
61 blooms (Hansen, 2002). Consequently, *S. costatum* experiences very severe CO₂ limitation
62 when blooms occur. To deal with it, *S. costatum* has developed multiple CCMs (Nimer *et al.*,
63 1998; Rost *et al.*, 2003). However, contrasting findings were reported. Nimer *et al.* (1998)
64 documented that extracellular carbonic anhydrase activity in *S. costatum* was only induced
65 when CO₂ concentration was less than 5 $\mu\text{mol L}^{-1}$ while Rost *et al.* (2003) reported that
66 activity of extracellular carbonic anhydrase could be detected even when CO₂ concentration
67 was 27 $\mu\text{mol L}^{-1}$. Chen and Gao (2004) showed that in *S. costatum* had little capacity in direct
68 HCO₃⁻ utilization. On the other hand, Rost *et al.* (2003) demonstrated that this species could

69 take up CO₂ and HCO₃⁻ simultaneously.

70 Phosphorus (P) is an indispensable element for all living organisms, serving as an integral
71 component of lipids, nucleic acids, ATP and a diverse range of other metabolites. Levels of
72 bioavailable phosphorus are very low in many ocean environments and phosphorus
73 enrichment can commonly increase algal growth and marine primary productivity in the
74 worldwide oceans (Davies & Sleep, 1989; Müller & Mitrovic, 2015; Lin *et al.*, 2016). Due to
75 the essential role of phosphorus, extensive studies have been conducted to investigate the
76 effect of phosphorus on photosynthetic performances (Geider *et al.*, 1998; Liu *et al.*, 2012;
77 Beamud *et al.*, 2016), growth (Jiang *et al.*, 2016; Reed *et al.*, 2016; Mccall *et al.*, 2017),
78 phosphorus acquisition, utilization and storage (Lin *et al.*, 2016; Gao *et al.*, 2018a). Some
79 studies show the essential role of phosphorus in regulating inorganic carbon acquisition in
80 green algae (Beardall *et al.*, 2005; Hu & Zhou, 2010). In terms of *S. costatum*, studies
81 regarding the inorganic carbon acquisition in *S. costatum* focus on its response to variation of
82 CO₂ availability. The role of phosphorus in *S. costatum*'s CCMs remains unknown. Based on
83 the connection between phosphorus and carbon metabolism in diatoms (Brembu *et al.*, 2017),
84 we hypothesize that phosphorus enrichment could enhance inorganic carbon utilization and
85 hence maintain high rates of photosynthesis and growth in *S. costatum* under CO₂ limitation
86 conditions. In the present study, we aimed to test this hypothesis by investigating the variation
87 of CCMs (including active transport of HCO₃⁻ and carbonic anhydrase activity) and
88 photosynthetic rate under five levels of phosphate and two levels of CO₂ conditions. We also
89 measured redox activity of plasma membrane as it is deemed to be critical to activate carbonic
90 anhydrase (Nimer *et al.*, 1998). Our study would provide helpful insights into how

91 bloom-forming diatoms overcome CO₂ limitation to maintain a quick growth rate during red
92 tides.

93 **2. Materials and Methods**

94 *2.1. Culture conditions*

95 *Skeletonema costatum* (Grev.) Cleve from Jinan University, China, was cultured in f/2
96 artificial seawater with five phosphate levels (0.05, 0.25, 1, 4, 10 μmol L⁻¹) by adding
97 different amounts of NaH₂PO₄ · 2H₂O. The cultures were carried out semi-continuously at
98 20°C for seven days. The light irradiance was set 200 μmol photons m⁻² s⁻¹, with a light and
99 dark period of 12: 12. The cultures were aerated with ambient air (0.3 L min⁻¹) to maintain the
100 pH around 8.2. The cells during exponential phase were collected and rinsed twice with
101 DIC-free seawater that was made according to Xu *et al.* (2017). Afterwards, cells were
102 resuspended in fresh media with two levels of pH (8.20 and 8.70, respectively corresponding
103 to ambient CO₂ (12.6 μmol L⁻¹, AC) and low CO₂ (2.8 μmol L⁻¹, LC) under corresponding
104 phosphate levels for two hours before the following measurements, with a cell density of 1.0
105 × 10⁶ mL⁻¹. Cell density was determined by direct counting with an improved Neubauer
106 haemocytometer (XB-K-25, Qiu Jing, Shanghai, China). This transfer aimed to investigate the
107 effects of phosphate on DIC acquisition under a CO₂ limitation condition. The pH of 8.70 was
108 chosen considering that it is commonly used as a CO₂ limitation condition (Nimer *et al.*, 1998;
109 Chen & Gao, 2004) and also occurs during algal bloom (Hansen, 2002). Two hours should be
110 enough to activate CCMs in *S. costatum* (Nimer *et al.*, 1998). The cell density did not vary
111 during the two hours of pH treatment. All experiments were conducted in triplicates.

112 *2.2. Manipulation of seawater carbonate system*

113 The two levels of pH (8.20 and 8.70) were obtained by aerating the ambient air and pure
114 nitrogen (99.999%) till the target value, and were then maintained with a buffer of 50 mM tris
115 (hydroxymethyl) aminomethane-HCl. The cultures were open to the ambient atmosphere and
116 the rise of culture pH was below 0.02 unites (corresponding to the rise of CO₂ less than 0.7
117 and 0.2 μmol L⁻¹ for pH 8.20 and 8.70 treatments respectively) during the two hours of pH
118 treatment. CO₂ level in seawater was calculated via CO2SYS (Pierrot *et al.*, 2006) based on
119 measured pH and TAlk, using the equilibrium constants of K1 and K2 for carbonic acid
120 dissociation (Roy *et al.*, 1993) and the KSO₄⁻ dissociation constant from Dickson (1990).

121 2.3. The pH_{NBS} was measured by a pH meter (pH 700, Eutech Instruments, Singapore) that
122 was equipped with an Orion[®] 8102BN Ross combination electrode (Thermo Electron Co.,
123 USA) and calibrated with standard National Bureau of Standards (NBS) buffers (pH =
124 4.01, 7.00, and 10.01 at 25.0 °C; Thermo Fisher Scientific Inc., USA). Total alkalinity
125 (TAlk) was determined at 25.0 °C by Gran acidimetric titration on a 25-ml sample with a
126 TAlk analyzer (AS-ALK1, Apollo SciTech, USA), using the precision pH meter and an
127 Orion[®] 8102BN Ross electrode for detection. To ensure the accuracy of TAlk, the TAlk
128 analyser was regularly calibrated with certified reference materials from Andrew G.
129 Dickson's laboratory (Scripps Institute of Oceanography, U.S.A.) at a precision of ± 2
130 μmol kg⁻¹. CO₂ level in seawater was calculated via CO2SYS (Pierrot *et al.*, 2006) based
131 on measured pH and TAlk, using the equilibrium constants of K1 and K2 for carbonic acid
132 dissociation (Roy *et al.*, 1993) and the KSO₄⁻ dissociation constant from Dickson (1990).

133 *Chlorophyll fluorescence measurement*

134 Chlorophyll fluorescence was measured with a pulse modulation fluorometer

135 (PAM-2100, Walz, Germany) to assess electron transport in photosystem II and the possible
136 connection between electron transport and redox activity of the plasma membrane. The
137 measuring light and actinic light were 0.01 and 200 $\mu\text{mol photons m}^{-2} \text{ s}^{-1}$, respectively. The
138 saturating pulse was set 4,000 $\mu\text{mol photons m}^{-2} \text{ s}^{-1}$ (0.8 s). Relative electron transport in
139 photosystem II (rETR, $\mu\text{mol e}^{-} \text{ m}^{-2} \text{ s}^{-1}$) = $(F_M' - F_t) / F_M' \times 0.5 \times \text{PFD}$ (Gao et al., 2018),
140 where F_M' is the maximal fluorescence levels from algae in the actinic light after application a
141 saturating pulse, F_t is the fluorescence at an excitation level and PFD is the actinic light
142 density.

143 2.4. Estimation of photosynthetic oxygen evolution and respiration

144 The net photosynthetic and respiration rates of *S. costatum* were measured using a
145 Clark-type oxygen electrode (YSI Model 5300, USA) that was held in a circulating water bath
146 (Cooling Circulator; Cole Parmer, Chicago, IL, USA) to keep the setting temperature (20°C).
147 Five mL of samples were transferred to the oxygen electrode cuvette and were stirred during
148 measurement. The light intensity and temperature were maintained as the same as that in the
149 growth condition. The illumination was provided by a halogen lamp. The increase of oxygen
150 content in seawater within five minutes was defined as net photosynthetic rate. To measure
151 dark respiration rate, the samples were placed in darkness and the decrease of oxygen content
152 within ten minutes was defined as dark respiration rate given the slower oxygen variation rate
153 for dark respiration. Net photosynthetic rate and dark respiration rate were presented as μmol
154 $\text{O}_2 (10^9 \text{ cells})^{-1} \text{ h}^{-1}$.

155 To obtain the curve of net photosynthetic rate versus DIC, seven levels of DIC (0, 0.1, 0.2,
156 0.5, 1, 2, and 4 mM) were made by adding different amounts of NaHCO_3 to the Tris buffered

157 DIC-free seawater (pH 8.20). The algal samples were washed twice with DIC-free seawater
158 before transferring to the various DIC solutions. Photosynthetic rates at different DIC levels
159 were measured under saturating irradiance of $400 \mu\text{mol photons m}^{-2} \text{ s}^{-1}$ and growth
160 temperature. The algal samples were allowed to equilibrate for 2–3 min at each DIC level
161 during which period a linear change in oxygen concentration was obtained and recorded. The
162 parameter, photosynthetic half saturation constant ($K_{0.5}$, i.e., the DIC concentration required to
163 give half of DIC-saturated maximum rate of photosynthetic O_2 evolution), was calculated
164 from the Michaelis-Menten kinetics equation (Caemmerer and Farquhar 1981): $V = V_{max} \times [S]$
165 $/ (K_{0.5} + [S])$, where V is the real-time photosynthetic rate, V_{max} is maximum photosynthetic
166 rate and $[S]$ is the DIC concentration. The value of $1/ K_{0.5}$ represents photosynthetic DIC
167 affinity. $K_{0.5}$ for CO_2 was calculated via CO2SYS (Pierrot *et al.*, 2006) based on pH and TA,
168 using the equilibrium constants of K1 and K2 for carbonic acid dissociation (Roy *et al.*, 1993)
169 and the KSO_4^- dissociation constant from Dickson (1990).

170 2.5. Measurement of photosynthetic pigment

171 To determine the photosynthetic pigment (Chl *a*) content, 50 mL of culture were filtered
172 on a Whatman GF/F filter, extracted in 5 mL of 90% acetone for 12 h at 4°C, and centrifuged
173 (3,000 g, 5 min). The optical density of the supernatant was scanned from 200 to 700 nm
174 with a UV-VIS spectrophotometer (Shimadzu UV-1800, Kyoto, Japan). The concentration of
175 Chl *a* was calculated based on the optical density at 630 and 664 nm: $\text{Chl } a = 11.47 \times \text{OD}_{664} -$
176 $0.40 \times \text{OD}_{630}$, $\text{Chl } c = 24.36 \times \text{OD}_{630} - 3.73 \times \text{OD}_{664}$ (Gao *et al.*, 2018b), and was normalized
177 to pg cells^{-1} .

178 2.6. Measurement of extracellular carbonic anhydrase activity

179 Carbonic anhydrase activity was assessed using the electrometric method (Gao *et al.*,
180 2009). Cells were harvested by centrifugation at 4, 000 g for five minutes at 20°C, washed
181 once and resuspended in 8 mL Na-barbital buffer (20 mM, pH 8.2). Five mL CO₂-saturated
182 icy distilled water was injected into the cell suspension, and the time required for a pH
183 decrease from 8.2 to 7.2 at 4°C was recorded. Extracellular carbonic anhydrase (CA_{ext})
184 activity was measured using intact cells. CA activity (E.U.) was calculated using the
185 following formula: E.U. = 10 × (T₀ / T - 1), where T₀ and T represent the time required for the
186 pH change in the absence or presence of the cells, respectively.

187 2.7. Measurement of redox activity in the plasma membrane

188 The redox activity of plasma membrane was assayed by monitoring the change in
189 K₃Fe(CN)₆ concentration that accompanied reduction of the ferricyanide to ferrocyanide. The
190 ferricyanide [K₃Fe(CN)₆] cannot penetrate intact cells and has been used as an external
191 electron acceptor (Nimer *et al.*, 1998; Wu & Gao, 2009). Stock solutions of K₃Fe(CN)₆ were
192 freshly prepared before use. Five mL of samples were taken after two hours of incubation
193 with 500 μmol K₃Fe(CN)₆ and centrifuged at 4000 g for 10 min (20°C). The concentration of
194 K₃Fe(CN)₆ in the supernatant was measured spectrophotometrically at 420 nm (Shimadzu
195 UV-1800, Kyoto, Japan). The decrease of K₃Fe(CN)₆ during the two hours of incubation
196 was used to assess the rate of extracellular ferricyanide reduction that was presented as μmol
197 (10⁶ cells)⁻¹ h⁻¹ (Nimer *et al.*, 1998).

198 2.8. Cell-driving pH drift experiment

199 To obtain the pH compensation point, the cells were transferred to sealed glass vials
200 containing fresh medium (pH 8.2) with corresponding phosphate levels. The cell

201 concentration for all treatments was $5.0 \times 10^5 \text{ mL}^{-1}$. The pH drift of the suspension was
202 monitored at 20°C and $200 \mu\text{mol photons m}^{-2} \text{ s}^{-1}$ light level. The pH compensation point was
203 obtained when there was no a further increase in pH.

204 2.9. Statistical analysis

205 Results were expressed as means of replicates \pm standard deviation and data were
206 analyzed using the software SPSS v.21. The data from each treatment conformed to a normal
207 distribution (Shapiro-Wilk, $P > 0.05$) and the variances could be considered equal (Levene's
208 test, $P > 0.05$). Two-way ANOVAs were conducted to assess the effects of CO_2 and phosphate
209 on net photosynthetic rate, dark respiration rate, ratio of net photosynthetic rate to dark
210 respiration rate, rETR, Chl *a*, $K_{0.5}$, CA_{ext} , reduction rate of ferricyanide, and pH compensation
211 point. Least Significant Difference (LSD) was conducted for *post hoc* investigation. Repeated
212 measures ANOVAs were conducted to analyze the effects of DIC on net photosynthetic rate
213 and the effect of incubation time on media pH in a closed system. Bonferroni was conducted
214 for *post hoc* investigation as it is the best reliable *post hoc* test for repeated measures ANOVA
215 (Ennos, 2007). The threshold value for determining statistical significance was $P < 0.05$.

216 3. Results

217 3.1. Effects of CO_2 and phosphate on photosynthetic and respiratory performances

218 The net photosynthetic rate and dark respiration rate in *S. costatum* grown at various CO_2
219 and phosphate concentrations were first investigated (Fig. 1). CO_2 interacted with phosphate
220 on net photosynthetic rate, with each factor having a main effect (Table 1). *Post hoc* LSD
221 comparison ($P = 0.05$) showed that LC reduced net photosynthetic rate when the phosphate
222 levels was below $4 \mu\text{mol L}^{-1}$ but did not affect it at the higher phosphate levels. Under AC, net

223 photosynthetic rate increased with phosphate level and reached the plateau (100.51 ± 9.59
224 $\mu\text{mol O}_2 (10^9 \text{ cells})^{-1} \text{ h}^{-1}$) at $1 \mu\text{mol L}^{-1}$ phosphate. Under LC, net photosynthetic rate also
225 increased with phosphate level but did not hit the peak ($101.46 \pm 9.19 \mu\text{mol O}_2 (10^9 \text{ cells})^{-1} \text{ h}^{-1}$)
226 until $4 \mu\text{mol L}^{-1}$ phosphate. In terms of dark respiration rate (Fig. 1b), phosphate had a main
227 effect on it and it interacted with CO_2 (Table 1). Specifically, LC increased dark respiration
228 rate at 0.05 and $0.25 \mu\text{mol L}^{-1}$ phosphate levels, but did not affect it when phosphate level was
229 above $1 \mu\text{mol L}^{-1}$ (LSD, $P < 0.05$). Regardless of CO_2 level, respiration rate increased with
230 phosphate availability and stopped at $1 \mu\text{mol L}^{-1}$.

231 The ratio of respiration to photosynthesis ranged from 0.23 to 0.40 (Fig. 2). Both CO_2 and
232 phosphate had a main effect, and they interacted on the ratio of respiration to photosynthesis
233 (Table 1). LC increased the ratio when phosphate was lower than $4 \mu\text{mol L}^{-1}$ but did not affect
234 it when phosphate levels were 4 or $10 \mu\text{mol L}^{-1}$.

235 Both CO_2 and phosphate affected rETR and they also showed an interactive effect (Fig. 3
236 & Table 2). For instance, *post hoc* LSD comparison showed that LC did not affect rETR at
237 lower phosphate levels (0.05 and $0.25 \mu\text{mol L}^{-1}$) but increased it at higher phosphate levels
238 (1 – $10 \mu\text{mol L}^{-1}$). Regardless of CO_2 treatment, rETR increased with phosphate level (0.05 – 4
239 $\mu\text{mol L}^{-1}$) but the highest phosphate concentration did not result in a further increase in rETR
240 (LSD, $P > 0.05$).

241 The content of Chl *a* was measured to investigate the effects of CO_2 and phosphate on
242 photosynthetic pigment in *S. costatum* (Fig. 4). Both CO_2 and phosphate affected the
243 synthesis of Chl *a* and they had an interactive effect (Table 2). *Post hoc* LSD comparison ($P =$
244 0.05) showed that LC did not affect Chl *a* at 0.05 or $0.25 \mu\text{mol L}^{-1}$ phosphate but stimulated

245 Chl *a* synthesis at higher phosphate levels (1–10 $\mu\text{mol L}^{-1}$). Irrespective of CO_2 treatment, Chl
246 *a* content increased with phosphate level and reached the plateau ($0.19 \pm 0.01 \text{ pg cell}^{-1}$ for AC
247 and $0.23 \pm 0.01 \text{ pg cell}^{-1}$ for LC) at 4 $\mu\text{mol L}^{-1}$ phosphate.

248 To assess the effects of CO_2 and phosphate on photosynthetic CO_2 affinity in *S. costatum*,
249 the net photosynthetic rates of cells exposure to seven levels of DIC were measured (Fig. 5).
250 After curve fitting, the values of $K_{0.5}$ for CO_2 were calculated (Fig. 6). CO_2 and phosphate
251 interplayed on $K_{0.5}$ and each had a main effect (Table 2). LC did not affect $K_{0.5}$ at the lowest
252 phosphate level but reduced it at the other phosphate levels. Under AC, higher phosphate
253 levels (0.25–4 $\mu\text{mol L}^{-1}$) reduced $K_{0.5}$ and the highest phosphate level led to a further decrease
254 to $2.59 \pm 0.29 \mu\text{mol kg}^{-1}$ seawater compared to the value of $4.00 \pm 0.30 \mu\text{mol kg}^{-1}$ seawater at
255 0.05 $\mu\text{mol L}^{-1}$ phosphate. The pattern with phosphate under LC was the same as the AC.

256 3.3. The effects of CO_2 and phosphate on inorganic carbon acquisition

257 To investigate the potential mechanisms that cells overcame CO_2 limitation during algal
258 blooms, the activity of CA_{ext} , a CCM related enzyme, was estimated under various CO_2 and
259 phosphate conditions (Fig. 7a). Both CO_2 and phosphate had a main effect and they interacted
260 on CA_{ext} activity (Table 3). *Post hoc* LSD comparison ($P = 0.05$) showed that LC induced
261 more CA_{ext} activity under all phosphate conditions except for 0.05 $\mu\text{mol L}^{-1}$ levels, compared
262 to AC. Under AC, CA_{ext} activity increased (0.04–0.10 EU (10^6 cells^{-1})) with phosphate level
263 and stopped increasing at 1 $\mu\text{mol L}^{-1}$ phosphate. Under LC, CA_{ext} activity also increased
264 (0.04–0.35 EU (10^6 cells^{-1})) with phosphate level but reached the peak at 4 $\mu\text{mol L}^{-1}$
265 phosphate. The redox activity of plasma membrane was also assessed to investigate the
266 factors that modulate CA_{ext} activity (Fig. 7b). The pattern of redox activity of plasma

267 membrane under various CO₂ and phosphate conditions was the same as that of CA_{ext} activity.
268 That is, CO₂ and phosphate had an interactive effect on redox activity of plasma membrane,
269 each having a main effect (Table 3).

270 To test cells' tolerance to high pH and obtain pH compensation points in *S. costatum*
271 grown under various CO₂ and phosphate levels, changes of media pH in a closed system were
272 monitored (Fig. 8). The media pH under all phosphate conditions increased with incubation
273 time (Table 4). Specifically speaking, there was a steep increase in pH during the first three
274 hours, afterwards the increase became slower and it reached a plateau in six hours (Bonferroni,
275 $P < 0.05$). Phosphate had an interactive effect with incubation time (Table 4). For instance,
276 there was no significant difference in media pH among phosphate levels during first two
277 hours of incubation but then divergence occurred and they stopped at different points.
278 Two-way ANOVA analysis showed that CO₂ treatment did not affect pH compensation point
279 but phosphate had a main effect (Table 3). Under each CO₂ treatment, pH compensation point
280 increased with phosphate level, with lowest of 9.03 ± 0.03 at $0.05 \mu\text{mol L}^{-1}$ and highest of
281 9.36 ± 0.04 at $10 \mu\text{mol L}^{-1}$ phosphate.

282 4. Discussion

283 4.1. Photosynthetic performances under various CO₂ and phosphate conditions

284 The lower CO₂ availability reduced the net photosynthetic rate of *S. costatum* grown at
285 the lower phosphate levels in the present study. However, Nimer *et al.* (1998) demonstrated
286 that the increase in pH (8.3–9.5) did not reduce photosynthetic CO₂ fixation of *S. costatum*
287 and Chen and Gao (2004) reported that a higher pH (8.7) even stimulated the photosynthetic
288 rate of *S. costatum* compared to the control (pH 8.2). The divergence between our and the

289 previous studies may be due to different nutrient supply. Both Nimer *et al.* (1998) and Chen
290 and Gao (2004) used f/2 media to grow algae. The phosphate concentration in f/2 media is
291 $\sim 36 \mu\text{mol L}^{-1}$, which is replete for physiological activities in *S. costatum*. *Skeletonema*
292 *costatum* grown at higher phosphate levels (4 and $10 \mu\text{mol L}^{-1}$) also showed similar
293 photosynthetic rates for the lower and higher CO₂ treatments. Our finding combined with the
294 previous studies indicates phosphorus plays an important role in dealing with low CO₂
295 availability for photosynthesis in *S. costatum*.

296 Different from net photosynthetic rate, LC did not affect rETR at lower phosphate levels
297 (0.05 and $0.25 \mu\text{mol L}^{-1}$) and stimulated it at higher phosphate levels ($1\text{--}10 \mu\text{mol L}^{-1}$). This
298 interactive effect of CO₂ and phosphate may be due to their effects on Chl *a*. LC induced
299 more synthesis of Chl *a* at higher phosphate levels ($1\text{--}10 \mu\text{mol L}^{-1}$). This induction of LC on
300 photosynthetic pigment is also reported in green algae (Gao *et al.*, 2016). More energy is
301 required under LC to address the more severe CO₂ limitation and thus more Chl *a* are
302 synthesized to capture more light energy, particularly when phosphate was replete. Although P
303 is not an integral component for chlorophyll, it plays an important role in cell energetics
304 through high-energy phosphate bonds, i.e. ATP, which could support chlorophyll synthesis.
305 The stimulating effect of P enrichment on photosynthetic pigment is also found in green alga
306 *Dunaliella tertiolecta* (Geider *et al.*, 1998) and brown alga *Sargassum muticum* (Xu *et al.*,
307 2017). The increased photosynthetic pigment in *S. costatum* could partially explain the
308 increased rETR and photosynthetic rate under the higher P conditions.

309 4.6. Ratio of respiration to photosynthesis

310 The ratio of respiration to photosynthesis in algae indicates carbon balance in cells and

311 carbon flux in marine ecosystems as well (Zou & Gao, 2013). LC increased this ratio in *S.*
312 *costatum* grown at the lower P conditions but did not affect it under the higher P conditions,
313 indicating that P enrichment can offset the carbon loss caused by carbon limitation. To cope
314 with CO₂ limitation, cells might have to obtain energy from dark respiration under lower P
315 conditions as it seems infeasible to acquire energy from the low rETR, which led to the
316 increased dark respiration. However, LC induced higher rETR under P replete conditions and
317 energy used for inorganic carbon (CO₂ and HCO₃⁻) acquisition could be from the increased
318 rETR. Therefore, additional dark respiration was not triggered, avoiding carbon loss. Most
319 studies regarding the effect of CO₂ on ratio of respiration to photosynthesis focus on higher
320 plants (Gifford, 1995; Ziska & Bunce, 1998; Cheng *et al.*, 2010; Smith & Dukes, 2013), little
321 is known on phytoplankton. Our study suggests that CO₂ limitation may lead to carbon loss in
322 phytoplankton but P enrichment could alter this trend, regulating carbon balance in
323 phytoplankton and thus their capacity in carbon sequestration.

324 *4.3. Inorganic carbon acquisition under CO₂ limitation and phosphate enrichment*

325 Decreased CO₂ can usually induce higher inorganic carbon affinity in algae (Raven *et al.*,
326 2012; Wu *et al.*, 2012; Raven *et al.*, 2017; Xu *et al.*, 2017). In the present study, the lower
327 CO₂ did increase inorganic carbon affinity when P level was higher than 0.25 μmol L⁻¹ but did
328 not affect it when P was 0.05 μmol L⁻¹, indicating the important role of P in regulating cells'
329 CCMs in response to environmental CO₂ changes. LC induced larger CA activity when P was
330 above 0.25 μmol L⁻¹ but did not increase it at 0.05 μmol L⁻¹ of P, which could explain the
331 interactive effect of P and CO₂ on inorganic carbon affinity as CA can accelerate the
332 equilibrium between HCO₃⁻ and CO₂ and increase inorganic carbon affinity. Regardless of

333 CO₂, P enrichment alone increased CA activity and inorganic carbon affinity. P enrichment
334 may stimulate the synthesis of CA by supplying required ATP. In addition, P enrichment
335 increased the redox activity of plasma membrane in this study. It has been proposed that redox
336 activity of plasma membrane could induce extracellular CA activity via protonation extrusion
337 of its active center (Nimer *et al.*, 1998). Our result that the pattern of CA is exactly same as
338 that of redox activity of plasma membrane shows a compelling correlation between CA and
339 redox activity of plasma membrane. The stimulating effect of P on redox activity of plasma
340 membrane may be due to its effect on rETR. The increased rETR could generate excess
341 reducing equivalents, particularly under CO₂ limiting conditions. These excess reducing
342 equivalents would be transported from the chloroplast into the cytosol (Heber, 1974),
343 supporting the redox chain in the plasma membrane (Rubinstein & Luster, 1993; Nimer *et al.*,
344 1999) and triggering CA activity.

345 4.4. Direct HCO₃⁻ utilization due to phosphate enrichment

346 A pH compensation point over 9.2 has been considered a sign of direct HCO₃⁻ use for
347 algae (Axelsson & Uusitalo, 1988) as the CO₂ concentration is nearly zero at pH above 9.2.
348 This criterion has been justified based on the experiments for both micro and macro-algae.
349 For instance, the marine diatom *Phaeodactylum tricornutum*, with a strong capacity for direct
350 HCO₃⁻ utilization, has a higher pH compensation point of 10.3 (Chen *et al.*, 2006). In contrast,
351 the red macroalgae, *Lomentaria articulata* and *Phycodryx rubens* that cannot utilize HCO₃⁻
352 directly and photosynthesis only depends on CO₂ diffusion, have pH compensation points of
353 less than 9.2 (Maberly, 1990). In terms of *S. costatum*, it has been reported to have a pH
354 compensation point of 9.12, indicating a very weak capacity in direct HCO₃⁻ utilization (Chen

355 & Gao, 2004). Our study demonstrates that the pH compensation point of *S. costatum* varies
356 with the availability of P. It is lower than 9.2 under P limiting conditions but higher than 9.2
357 under P replete conditions, suggesting that the capacity of direct HCO_3^- utilization is regulated
358 by P availability. Contrary to CO_2 passive diffusion, the direct use of HCO_3^- depends on
359 positive transport that requires energy (Hopkinson & Morel, 2011). P enrichment increased
360 rETR in the present study and the ATP produced during the process of electron transport could
361 be used to support HCO_3^- positive transport. In addition, the increased respiration at higher P
362 levels can also generate ATP to help HCO_3^- positive transport. Our study indicates that P
363 enrichment could trigger HCO_3^- direct utilization and hence increase inorganic acquisition
364 capacity of *S. costatum* to cope with CO_2 limitation.

365 4.5. CCMs and red tides

366 With the development of red tides, the pH in seawater could be very high along with
367 extremely low CO_2 availability due to intensive photosynthesis (Hansen, 2002; Hinga, 2002).
368 For instance, pH level in the surface waters of the eutrophic Mariager Fjord, Denmark, is
369 often above 9 during dinoflagellate blooms (Hansen, 2002). Diatoms are the casautive species
370 for red tides and *S. costatum* could outcompete other bloom algae (dinoflagellates
371 *Prorocentrum minimum* and *Alexandrium tamarense*) under nutrient replete conditions (Hu *et*
372 *al.*, 2011). However, the potential mechanisms are poorly understood. Our study demonstrates
373 *S. costatum* has multiple CCMs to cope with CO_2 limitation and the operation of CCMs is
374 regulated by P availability. The CCMs of *S. costatum* are hampered under P limiting
375 conditions and only function when P is replete. Therefore, P enrichment would be critical for
376 *S. costatum* to overcome carbon limitation during algal bloom and to dominate red tides.

377 **5. Conclusions**

378 The present study investigated the role of P in regulating inorganic carbon acquisition and
379 CO₂ concentrating mechanisms in diatoms for the first time. The intensive photosynthesis and
380 quick growth during algal blooms usually result in noticeable increase of pH and decrease of
381 CO₂. Our study demonstrates that P enrichment could induce activity of extracellular carbonic
382 anhydrase and direct utilization of HCO₃⁻ in *S. costatum* to help overcome the CO₂ limitation,
383 as well as increasing photosynthetic pigment content and rETR to provide required energy.
384 This study provides important insight into the connection of phosphorus and carbon
385 acquisition in diatoms and the mechanisms that *S. costatum* dominates algal blooms.

386 **Author contribution**

387 JX and GG designed the experiments, and GG, JY, JF and XZ carried them out. GG
388 prepared the manuscript with contributions from all co-authors.

389 **Acknowledgements**

390 This work was supported by National Natural Science Foundation of China (No.
391 41376156 & 40976078), Natural Science Fund of Guangdong Province (No.
392 S2012010009853), Science and Technology Bureau of Lianyungang (SH1606), Jiangsu
393 Planned Projects for Postdoctoral Research Funds (1701003A), Science Foundation of
394 Huaihai Institute of Technology (Z2016007), and
395 Foundation for High-level Talents in Higher Education of Guangdong.

396 **References**

397 **Anderson DM, Burkholder JM, Cochlan WP, Glibert PM, Gobler CJ, Heil CA, Kudela**
398 **R, Parsons ML, Rensel JE, Townsend DW. 2008.** Harmful algal blooms and

-
- 399 eutrophication: Examining linkages from selected coastal regions of the United States.
400 *Harmful Algae* **8**: 39-53.
- 401 **Axelsson L, Uusitalo J. 1988.** Carbon acquisition strategies for marine macroalgae. *Marine*
402 *Biology* **97**: 295-300.
- 403 **Barton AD, Irwin AJ, Finkel ZV, Stock CA. 2016.** Anthropogenic climate change drives
404 shift and shuffle in North Atlantic phytoplankton communities. *Proceedings of the*
405 *National Academy of Sciences, USA* **113**: 2964-2969.
- 406 **Beamud SG, Baffico GD, Reid B, Torres R, Gonzalez-Polo M, Pedrozo F, Diaz M. 2016.**
407 Photosynthetic performance associated with phosphorus availability in mats of
408 *Didymosphenia geminata* (Bacillariophyceae) from Patagonia (Argentina and Chile).
409 *Phycologia* **55**: 118-125.
- 410 **Beardall J, Roberts S, Raven JA. 2005.** Regulation of inorganic carbon acquisition by
411 phosphorus limitation in the green alga *Chlorella emersonii*. *Canadian Journal of*
412 *Botany* **83**: 859-864.
- 413 **Berg GM, Glibert PM, Lomas MW, Burford MA. 1997.** Organic nitrogen uptake and
414 growth by the chrysophyte *Aureococcus anophagefferens* during a brown tide event.
415 *Marine Biology* **129**: 377-387.
- 416 **Brembu T, Mühlroth A, Alipanah L, Bones AM. 2017.** The effects of phosphorus limitation
417 on carbon metabolism in diatoms. *Philosophical Transactions of the Royal Society B*
418 *Biological Sciences* **372**: 20160406.
- 419 **Bruland KW, Rue EL, Smith GJ. 2001.** Iron and macronutrients in California coastal
420 upwelling regimes: implications for diatom blooms. *Limnology and Oceanography* **46**:

-
- 421 1661-1674.
- 422 **Caemmerer SV, Farquhar GD. 1981.** Some relationships between the biochemistry of
423 photosynthesis and the gas exchange of leaves. *Planta* 153: 376-387.
- 424 **Chen X, Gao K. 2004.** Photosynthetic utilisation of inorganic carbon and its regulation in the
425 marine diatom *Skeletonema costatum*. *Functional Plant Biology* **31**: 1027-1033.
- 426 **Chen X, Qiu CE, Shao JZ. 2006.** Evidence for K⁺-dependent HCO₃⁻ utilization in the marine
427 diatom *Phaeodactylum tricornutum*. *Plant Physiology* **141**: 731-736.
- 428 **Cheng W, Sims DA, Luo Y, Coleman JS, Johnson DW. 2010.** Photosynthesis, respiration,
429 and net primary production of sunflower stands in ambient and elevated atmospheric
430 CO₂ concentrations: an invariant NPP:GPP ratio? *Global Change Biology* **6**: 931-941.
- 431 **Davies AG, Sleep JA. 1989.** The photosynthetic response of nutrient-depleted dilute cultures
432 of *Skeletonema costatum* to pulses of ammonium and nitrate; the importance of
433 phosphate. *Journal of Plankton Research* **11**: 141-164.
- 434 **Dickson AG. 1990.** Standard potential of the reaction: AgCl(s) + 12H₂(g) = Ag(s) + HCl(aq),
435 and the standard acidity constant of the ion HSO₄⁻ in synthetic sea water from 273.15
436 to 318.15 K. *Journal of Chemical Thermodynamics* **22**: 113-127.
- 437 **Ennos AR. 2017.** Statistical and Data Handling Skills in Biology. Pearson Education, p.96.
- 438 **Falkowski P. 2012.** Ocean Science: The power of plankton. *Nature* **483**: 17-20.
- 439 **Field CB, Behrenfeld MJ, Randerson JT, Falkowski P. 1998.** Primary production of the
440 biosphere: integrating terrestrial and oceanic components. *Science* **281**: 237-240.
- 441 **Gao G, Clare AS, Rose C, Caldwell GS. 2018a.** *Ulva rigida* in the future ocean: potential
442 for carbon capture, bioremediation, and biomethane production. *Global Change*
443 *Biology Bioenergy* **10**: 39-51.

-
- 444 **Gao G, Gao K, Giordano M. 2009.** Responses to solar UV radiation of the diatom
445 *Skeletonema costatum* (Bacillariophyceae) grown at different Zn^{2+} concentrations
446 *Journal of Phycology* **45**: 119-129.
- 447 **Gao G, Liu Y, Li X, Feng Z, Xu J. 2016.** An ocean acidification acclimatised green tide alga
448 Is robust to changes of seawater carbon chemistry but vulnerable to light stress. *PloS*
449 *One* **11**: e0169040.
- 450 **Gao G, Xia J, Yu J, Zeng X. 2018b.** Physiological response of a red tide alga (*Skeletonema*
451 *costatum*) to nitrate enrichment, with special reference to inorganic carbon acquisition.
452 *Marine Environmental Research*, **133**: 15-23.
- 453 **Geider RJ, Macintyre HL, Graziano LM, McKay RML. 1998.** Responses of the
454 photosynthetic apparatus of *Dunaliella tertiolecta* (Chlorophyceae) to nitrogen and
455 phosphorus limitation. *European Journal of Phycology* **33**: 315-332.
- 456 **Gifford RM. 1995.** Whole plant respiration and photosynthesis of wheat under increased CO_2
457 concentration and temperature: long-term vs. short-term distinctions for modelling.
458 *Global Change Biology* **1**: 385–396.
- 459 **Hansen PJ. 2002.** Effect of high pH on the growth and survival of marine phytoplankton:
460 implications for species succession. *Aquatic Microbial Ecology* **28**: 279-288.
- 461 **Heber U. 1974.** Metabolite exchange between chloroplasts and cytoplasm. *Annual Review of*
462 *Plant Physiology* **25**: 393-421.
- 463 **Hinga KR. 2002.** Effects of pH on coastal marine phytoplankton. *Marine Ecology Progress*
464 *Series* **238**: 281-300.
- 465 **Hopkinson BM, Dupont CL, Matsuda Y. 2016.** The physiology and genetics of CO_2

-
- 466 concentrating mechanisms in model diatoms. *Current Opinion in Plant Biology* **31**:
467 51-57.
- 468 **Hopkinson BM, Morel FMM. 2011.** Efficiency of the CO₂-concentrating mechanism of
469 diatoms. *Proceedings of the National Academy of Sciences, USA* **108**: 3830-3837.
- 470 **Hu H, Zhang J, Chen W. 2011.** Competition of bloom-forming marine phytoplankton at low
471 nutrient concentrations. *Journal of Environmental Sciences* **23**: 656-663.
- 472 **Hu H, Zhou Q. 2010.** Regulation of inorganic carbon acquisition by nitrogen and phosphorus
473 levels in the *Nannochloropsis* sp. *World Journal of Microbiology & Biotechnology* **26**:
474 957-961.
- 475 **Jeong HJ, An SL, Franks PJS, Lee KH, Ji HK, Kang NS, Lee MJ, Jang SH, Lee SY,**
476 **Yoon EY. 2015.** A hierarchy of conceptual models of red-tide generation: Nutrition,
477 behavior, and biological interactions. *Harmful Algae* **47**: 97-115.
- 478 **Jiang X, Han Q, Gao X, Gao G. 2016.** Conditions optimising on the yield of biomass, total
479 lipid, and valuable fatty acids in two strains of *Skeletonema menzeli*. *Food Chemistry*
480 **194**: 723-732.
- 481 **Li G, Gao K, Yuan D, Zheng Y, Yang G. 2011.** Relationship of photosynthetic carbon
482 fixation with environmental changes in the Jiulong River estuary of the South China
483 Sea, with special reference to the effects of solar UV radiation. *Marine Pollution*
484 *Bulletin* **62**: 1852-1858.
- 485 **Lin S, Litaker RW, Sunda WG. 2016.** Phosphorus physiological ecology and molecular
486 mechanisms in marine phytoplankton. *Journal of Phycology* **52**: 10.
- 487 **Liu Y, Song X, Cao X, Yu Z. 2012.** Responses of photosynthetic characters of *Skeletonema*

-
- 488 *costatum* to different nutrient conditions. *Journal of Plankton Research* **35**: 165-176.
- 489 **Maberly SC. 1990.** Exogenous sources of inorganic carbon for photosynthesis by marine
490 macroalgae. *Journal of Phycology* **26**: 439-449.
- 491 **Mccall SJ, Hale MS, Smith JT, Read DS, Bowes MJ. 2017.** Impacts of phosphorus
492 concentration and light intensity on river periphyton biomass and community structure.
493 *Hydrobiologia* **792**: 315-330.
- 494 **Moore CM, Mills MM, Arrigo KR, Bermanfrank I, Bopp L, Boyd PW, Galbraith ED,**
495 **Geider RJ, Guieu C, Jaccard SL. 2013.** Processes and patterns of oceanic nutrient
496 limitation. *Nature Geoscience* **6**: 701-710.
- 497 **Müller S, Mitrovic SM. 2015.** Phytoplankton co-limitation by nitrogen and phosphorus in a
498 shallow reservoir: progressing from the phosphorus limitation paradigm.
499 *Hydrobiologia* **744**: 255-269.
- 500 **Nelson DM, Tréguer P, Brzezinski MA, Leynaert A, Quéguiner B. 1995.** Production and
501 dissolution of biogenic silica in the ocean: Revised global estimates, comparison with
502 regional data and relationship to biogenic sedimentation. *Global Biogeochemical*
503 *Cycles* **9**: 359-372.
- 504 **Nimer NA, Ling MX, Brownlee C, Merrett MJ. 1999.** Inorganic carbon limitation,
505 exofacial carbonic anhydrase activity, and plasma membrane redox activity in marine
506 phytoplankton species. *Journal of Phycology* **35**: 1200-1205.
- 507 **Nimer NA, Warren M, Merrett MJ. 1998.** The regulation of photosynthetic rate and
508 activation of extracellular carbonic anhydrase under CO₂-limiting conditions in the
509 marine diatom *Skeletonema costatum*. *Plant Cell and Environment* **21**: 805–812.

-
- 510 **Pierrot D, Lewis E, Wallace DWR. 2006.** MS Excel program developed for CO₂ system
511 calculations. *ORNL/CDIAC-105a. Carbon Dioxide Information Analysis Center, Oak*
512 *Ridge National Laboratory, US Department of Energy, Oak Ridge, Tennessee.*
- 513 **Raven JA, Beardall J, Sánchez-Baracaldo P. 2017.** The possible evolution, and future, of
514 CO₂-concentrating mechanisms. *Journal of Experimental Botany.*
- 515 **Raven JA, Giordano M, Beardall J, Maberly SC. 2012.** Algal evolution in relation to
516 atmospheric CO₂: carboxylases, carbon-concentrating mechanisms and carbon
517 oxidation cycles. *Phil. Trans. R. Soc. B* **367**: 493-507.
- 518 **Reed ML, Pinckney JL, Keppler CJ, Brock LM, Hogan SB, Greenfield DI. 2016.** The
519 influence of nitrogen and phosphorus on phytoplankton growth and assemblage
520 composition in four coastal, southeastern USA systems. *Estuarine Coastal & Shelf*
521 *Science* **177**: 71-82.
- 522 **Rost B, Riebesell U, Burkhardt S, Sültemeyer D. 2003.** Carbon acquisition of
523 bloom-forming marine phytoplankton. *Limnology and Oceanography* **48**: 55-67.
- 524 **Roy RN, Roy LN, Vogel KM, Porter-Moore C, Pearson T, Good CE, Millero FJ,**
525 **Campbell DM. 1993.** The dissociation constants of carbonic acid in seawater at
526 salinities 5 to 45 and temperatures 0 to 45°C. *Marine Chemistry* **44**: 249-267.
- 527 **Rubinstein B, Luster DG. 1993.** Plasma membrane redox activity: components and role in
528 plant processes. *Annual Review of Plant Biology* **44**: 131-155.
- 529 **Smetacek V, Zingone A. 2013.** Green and golden seaweed tides on the rise. *Nature* **504**:
530 84-88.
- 531 **Smith NG, Dukes JS. 2013.** Plant respiration and photosynthesis in global-scale models:

-
- 532 incorporating acclimation to temperature and CO₂. *Global Change Biology* **19**: 45-63.
- 533 **Wang J. 2002.** Phytoplankton communities in three distinct ecotypes of the Changjiang
534 estuary. *Journal of Ocean University of China* **32**: 422-428.
- 535 **Wu H, Gao K. 2009.** Ultraviolet radiation stimulated activity of extracellular carbonic
536 anhydrase in the marine diatom *Skeletonema costatum*. *Functional Plant Biology* **36**:
537 137-143.
- 538 **Wu X, Gao G, Giordano M, Gao K. 2012.** Growth and photosynthesis of a diatom grown
539 under elevated CO₂ in the presence of solar UV radiation. *Fundamental and Applied*
540 *Limnology* **180**: 279-290.
- 541 **Xu Z, Gao G, Xu J, Wu H. 2017.** Physiological response of a golden tide alga (*Sargassum*
542 *muticum*) to the interaction of ocean acidification and phosphorus enrichment.
543 *Biogeosciences* **14**: 671-681.
- 544 **Young JN, Morel FMM. 2015.** Biological oceanography: The CO₂ switch in diatoms. *Nature*
545 *Climate Change* **5**: 722-723.
- 546 **Ziska LH, Bunce JA. 1998.** The influence of increasing growth temperature and CO₂
547 concentration on the ratio of respiration to photosynthesis in soybean seedlings.
548 *Global Change Biology* **4**: 637-643.
- 549 **Zou D, Gao K. 2013.** Thermal acclimation of respiration and photosynthesis in the marine
550 macroalga *Gracilaria lemaneiformis* (Gracilariales, Rhodophyta). *Journal of*
551 *Phycology* **49**: 61-68.

552

553

554 Table 1 Two-way analysis of variance for the effects of CO₂ and phosphate on net
 555 photosynthetic rate, dark respiration rate and ratio of respiration to photosynthesis of *S.*
 556 *costatum*. CO₂*phosphate means the interactive effect of CO₂ and phosphate, df means degree
 557 of freedom, F means the value of F statistic, and Sig. means p-value.

558

Source	Net photosynthetic rate			Dark respiration rate			Ratio of respiration to photosynthesis		
	df	F	Sig.	df	F	Sig.	df	F	Sig.
CO ₂	1	11.286	0.003	1	1.262	0.275	1	32.443	<0.001
Phosphate	4	157.925	<0.001	4	169.050	<0.001	4	7.081	0.001
CO ₂ *phosphate	4	3.662	0.021	4	3.226	0.034	4	8.299	<0.001
Error	20			20			20		

559 Table 2 Two-way analysis of variance for the effects of CO₂ and phosphate on relative
 560 electron transport rate (rETR), Chl *a*, and CO₂ level required to give half of DIC-saturated
 561 maximum rate of photosynthetic O₂ evolution ($K_{0.5}$) of *S. costatum*. CO₂*phosphate means the
 562 interactive effect of CO₂ and phosphate, df means degree of freedom, F means the value of F
 563 statistic, and Sig. means p-value.

564

Source	rETR			Chl <i>a</i>			$K_{0.5}$		
	df	F	Sig.	df	F	Sig.	df	F	Sig.
CO ₂	1	28.717	<0.001	1	32.963	<0.001	1	96.182	<0.001
Phosphate	4	127.860	<0.001	4	92.045	<0.001	4	40.497	<0.001
CO ₂ *phosphate	4	3.296	0.031	4	3.871	0.017	4	3.821	0.018
Error	20			20			20		

565 Table 3 Two-way analysis of variance for the effects of CO₂ and phosphate on CA_{ext} activity,
 566 redox activity of plasma membrane and pH compensation point of *S. costatum*.
 567 CO₂*phosphate means the interactive effect of CO₂ and phosphate, df means degree of
 568 freedom, F means the value of F statistic, and Sig. means p-value.

569

Source	CA _{ext} activity			redox activity of plasma membrane			pH compensation point		
	df	F	Sig.	df	F	Sig.	df	F	Sig.
CO ₂	1	569.585	<0.001	1	937.963	<0.001	1	0.056	0.816
Phosphate	4	176.392	<0.001	4	276.362	<0.001	4	226.196	<0.001
CO ₂ *phosphate	4	87.380	<0.001	4	137.050	<0.001	4	0.040	0.997
Error	20			20			20		

570 Table 4 Repeated measures analysis of variance for the effects of CO₂ and phosphate on pH
 571 change during 10 hours of incubation. Time*CO₂ means the interactive effect of incubation
 572 time and CO₂, Time*phosphate means the interactive effect of incubation time and phosphate,
 573 Time*CO₂*phosphate means the interactive effect of incubation time, CO₂ and phosphate,
 574 df means degree of freedom, F means the value of F statistic, and Sig. means p-value.

Source	Type III Sum of Squares	df	Mean Square	F	Sig.
Time	40.766	10	4.077	8737.941	<0.001
Time*CO ₂	0.003	10	<0.001	0.569	0.838
Time*phosphate	0.886	40	0.022	47.496	<0.001
Time*CO ₂ *phosphate	0.002	40	<0.001	0.112	1.000
Error	0.093	200	<0.001		

Figure legends

Fig. 1. Net photosynthetic rate (a) and dark respiration rate (b) in *S. costatum* grown at various phosphate concentrations after ambient (AC) and low CO₂ (LC) treatments. The error bars indicate the standard deviations (n = 3). Different letters represent the significant difference ($P < 0.05$) among phosphate concentrations (capital for AC, lower case for LC). Horizontal lines represent significant difference ($P < 0.05$) between CO₂ treatments.

Fig. 2. Ratio of respiration rate to net photosynthetic rate in *S. costatum* grown at various phosphate concentrations after ambient (AC) and low CO₂ (LC) treatments. The error bars indicate the standard deviations (n = 3). Different letters represent the significant difference ($P < 0.05$) among phosphate concentrations (capital for AC, lower case for LC). Horizontal lines represent significant difference ($P < 0.05$) between CO₂ treatments.

Fig. 3. Relative electron transport rate (rETR) in *S. costatum* grown at various phosphate concentrations after ambient (AC) and low CO₂ (LC) treatments. The error bars indicate the standard deviations (n = 3). Different letters represent the significant difference ($P < 0.05$) among phosphate concentrations (Capital for AC lower case for LC). Horizontal lines represent significant difference ($P < 0.05$) between CO₂ treatments.

Fig. 4. Photosynthetic Chl *a* content in *S. costatum* grown at various phosphate concentrations after ambient (AC) and low CO₂ (LC) treatments. The error bars indicate the standard deviations (n = 3). Different letters represent the significant difference ($P < 0.05$) among phosphate concentrations (capital for AC, lower case for LC). Horizontal lines represent significant difference ($P < 0.05$) between CO₂ treatments.

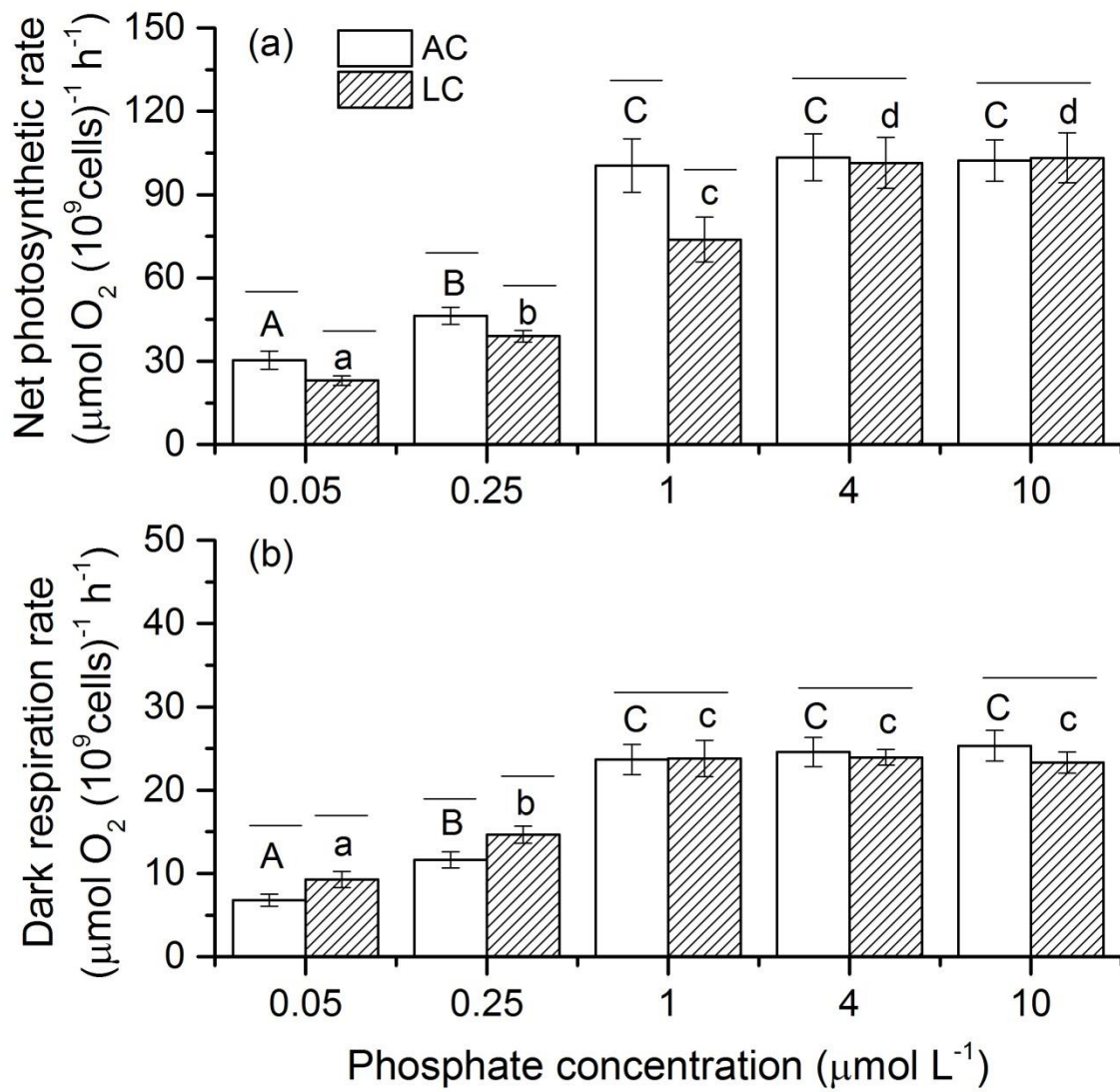
Fig. 5. Net photosynthetic rate as a function of DIC for *S. costatum* grown at various

597 phosphate concentrations after ambient (a) and low CO₂ (b) treatments. The error bars
598 indicate the standard deviations (n = 3).

599 **Fig. 6.** Half saturation constant ($K_{0.5}$) for CO₂ in *S. costatum* grown at various phosphate
600 concentrations after ambient (AC) and low CO₂ (LC) treatments. The error bars indicate the
601 standard deviations (n = 3). Different letters represent the significant difference ($P < 0.05$)
602 among phosphate concentrations (capital for AC, lower case for LC). Horizontal lines
603 represent significant difference ($P < 0.05$) between CO₂ treatments.

604 **Fig. 7.** CA_{ext} activity (a) and reduction rate of ferricyanide (b) in *S. costatum* grown at various
605 phosphate concentrations after ambient (AC) and low CO₂ (LC) treatments. The error bars
606 indicate the standard deviations (n = 3). Different letters represent the significant difference (P
607 < 0.05) among phosphate concentrations (capital for AC, lower case for LC). Horizontal lines
608 represent significant difference ($P < 0.05$) between CO₂ treatments.

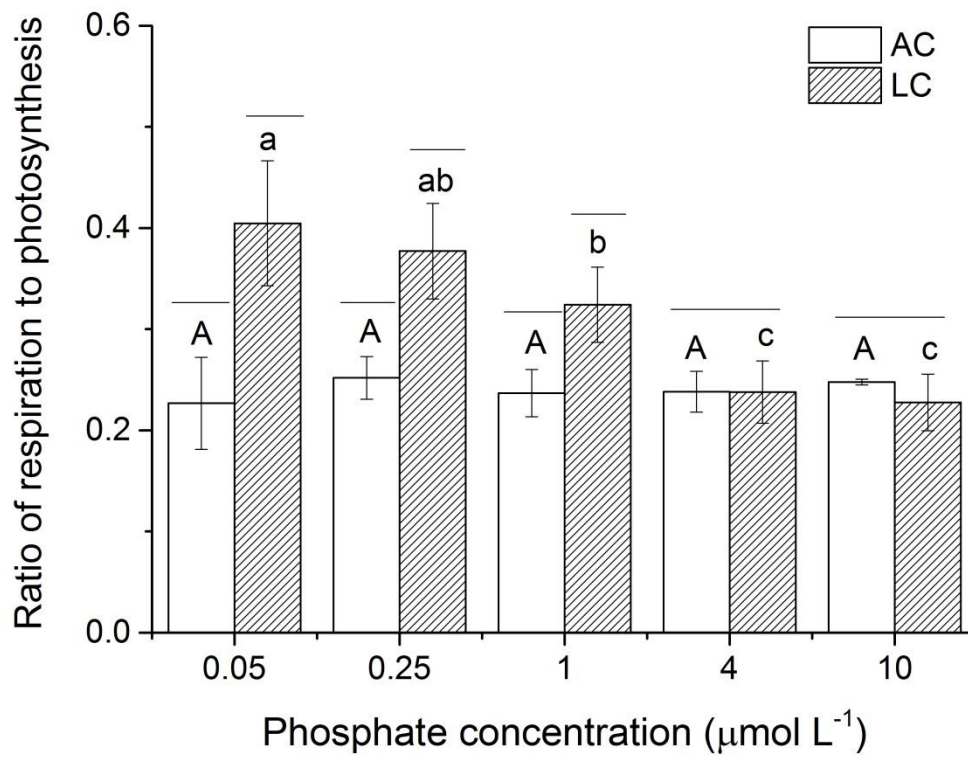
609 **Fig. 8.** Changes of pH in a closed system caused by photosynthesis of *S. costatum* grown at
610 various phosphate concentrations after ambient (AC) and low CO₂ (LC) treatments. The error
611 bars indicate the standard deviations (n = 3).



612

613

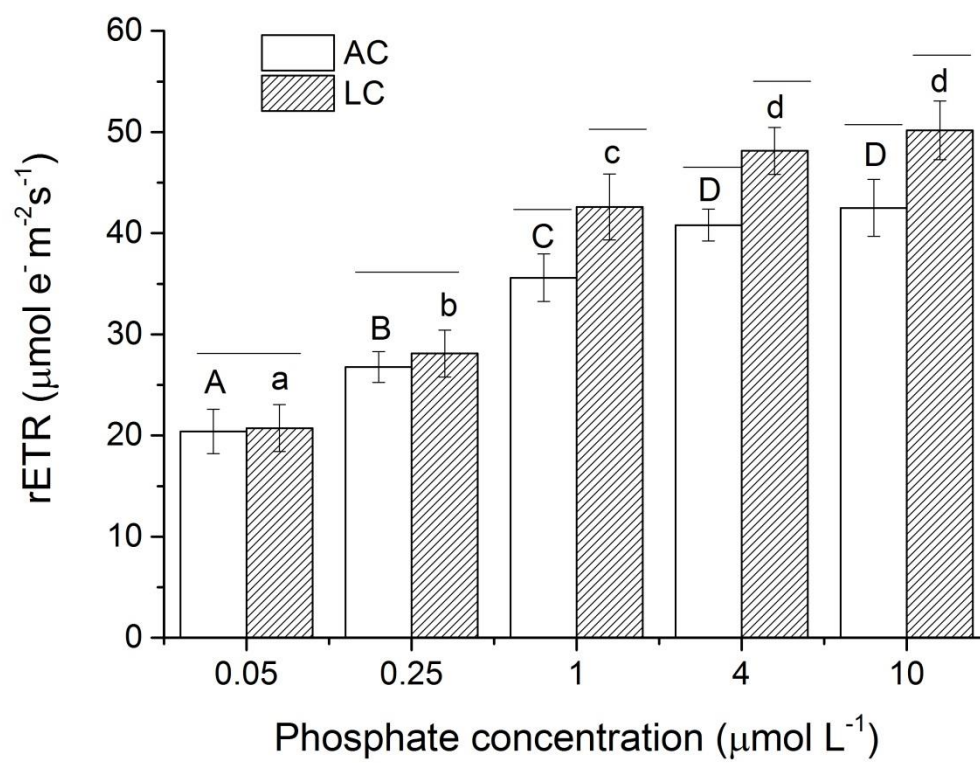
Fig. 1



614

615

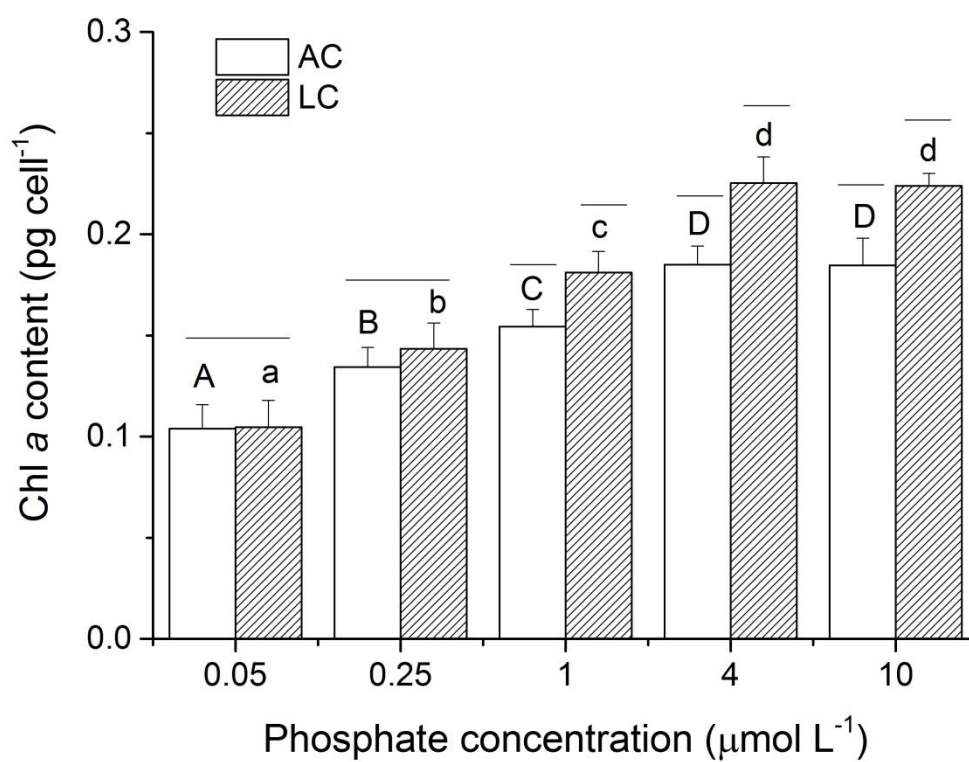
Fig. 2



616

617

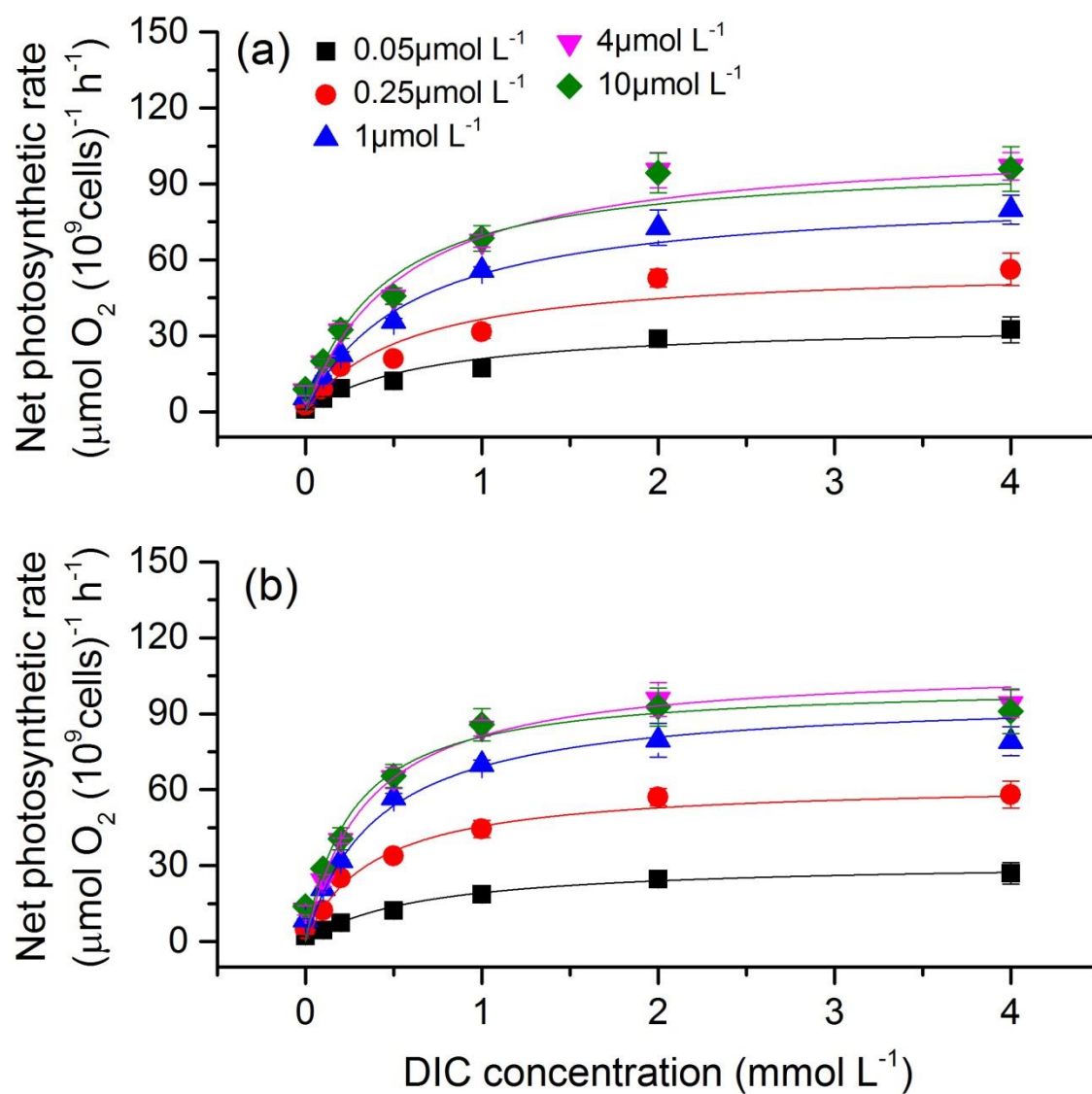
Fig. 3



618

619

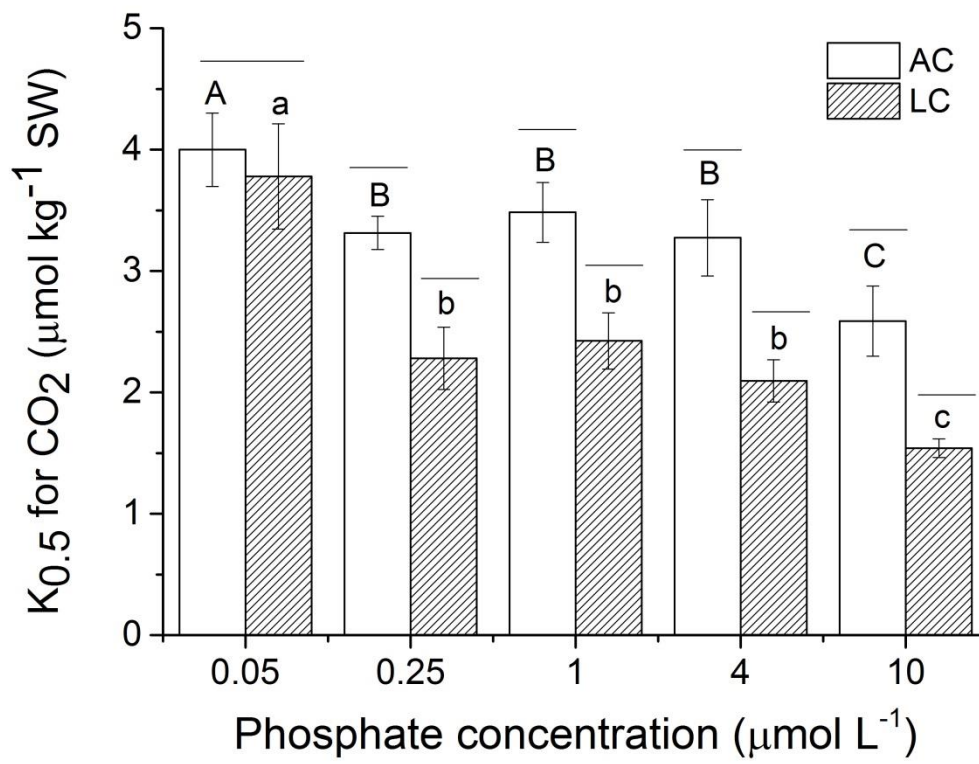
Fig. 4



620

621

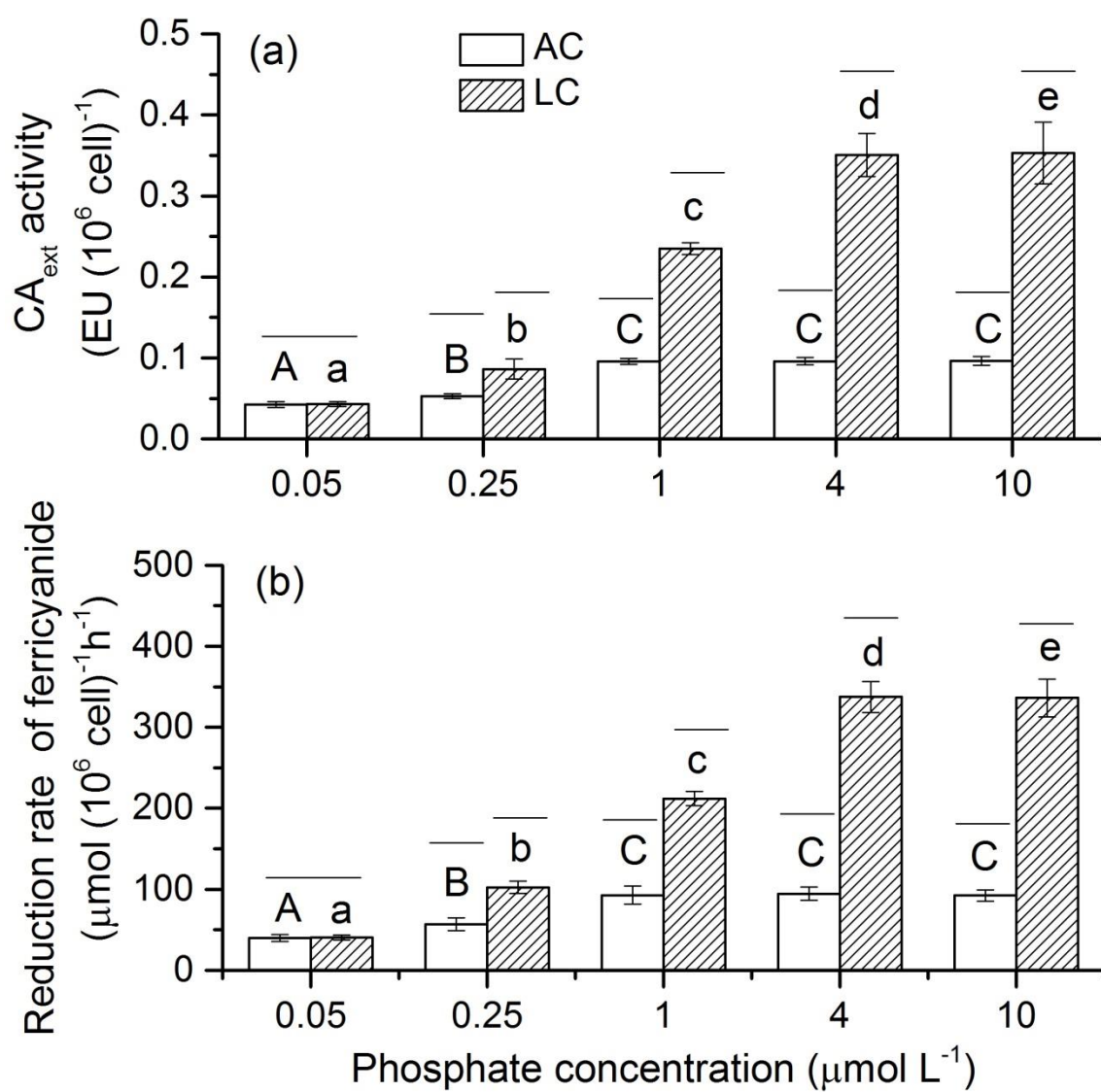
Fig. 5



622

623

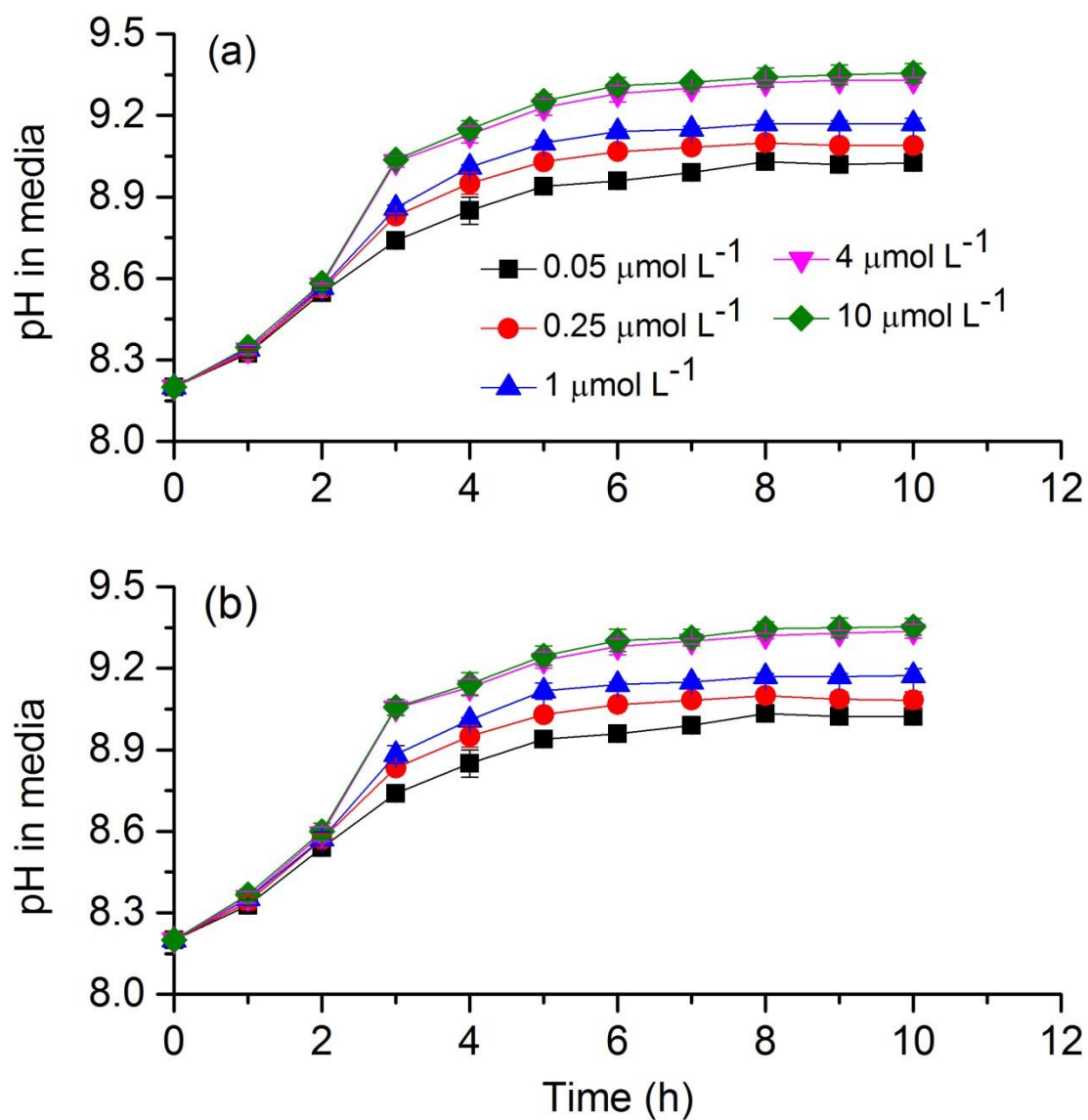
Fig. 6



624

625

Fig. 7



626

627

628

629

Fig. 8